Vol.66: e23220896, 2023
https://doi.org/10.1590/1678-4324-2023220896
ISSN 1678-4324 Online Edition

Article - Engineering, Technology and Techniques

Equilibrium Optimization Algorithm with Deep Learning Based Brain Tumor Segmentation and Classification on Magnetic Resonance Imaging

Hariharan Ramamoorthy[1*]
https://orcid.org/0000-0003-4198-765X

Mohan Ramasundaram[2]
http://orcid.org/ 0000-0002-3710-6808

Raja Soosaimarian Peter Raj[3]
https://orcid.org/0000-0002-7216-2207

Krunal Randive[4]
https://orcid.org/ 0000-0002-5728-701X

[1]National Institute of Technology, Department of Computer Science and Engineering, Tiruchirappalli , Tamilnadu, India; [2]National Institute of Technology, Department of Computer Science and Engineering, Tiruchirappalli , Tamilnadu, India; [3]Vellore Institute of Technology, School of Computer Science and Engineering, Vellore, Tamil Nadu, India; [4]National Institute of Technology, Department of Computer Science and Engineering, Tiruchirappalli , Tamilnadu, India;

Editor-in-Chief: Alexandre Rasi Aoki
Associate Editor: Fabio Alessandro Guerra

Received: 05-Dec-2022; Accepted: 05-Jun-2023

*Correspondence: hharanbtech@gmail.com (H.R.).

HIGHLIGHTS

- Proposed an EOADL-BTSC technique for Brain Tumor Segmentation and Classification.
- Perform data preprocessing in two stages namely CLAHE based contrast enhancement and skull stripping.
- Developed EOA with Attention inception based UNet technique is developed for medical image segmentation.
- Employ CapsNet based feature extraction and CRNN model for brain disorder classification.

Abstract: Brain tumors (BTs) are a serious medical condition that can have significant impacts on individuals. These tumors typically originate in various parts of the brain and can be detected using Magnetic Resonance Imaging (MRI), which has become an essential tool for medical research. However, manual analysis of MRI images for BT segmentation is a time-consuming and error-prone process. To address this challenge, automated methods based on deep learning algorithms have been developed for fast and accurate detection of anomalous brain regions. In this article, we propose a novel approach called Equilibrium Optimizer Algorithm with Deep Learning-based Brain Tumor Segmentation and Classification (EOADL-BTSC) for brain tumor segmentation and classification using MRI images. Our method uses enhancement of contrast and skull stripping to preprocess the images, followed by an attention-inception-based UNet model for

segmentation, a capsule network (CapsNet) model for feature extraction, and a cascaded recurrent neural network (CRNN) for classification. To optimize the performance of our proposed method, we use the Equilibrium Optimizer Algorithm (EOA) to fine-tune the hyperparameters of the UNet model. We evaluate the performance of our approach on a benchmark database and compare it with other recent approaches. Our experimental results demonstrate that the EOADL-BTSC methodology outperforms the other approaches in terms of several performance measures. In summary, the proposed DL-BTSC methodology provides a promising solution for automated brain tumor segmentation and classification using MRI images. It has the potential to assist medical professionals in accurate and fast detection of brain tumors, leading to better medical analysis and treatment planning. Our proposed method achieves the maximum accu_y, sens_y, and spec_y values of 99.15% 98.78%, and 99.15% respectively. They also note that the proposed approach requires fewer parameters and has a quicker segmentation time than previous approaches.

Keywords: Brain tumor; Deep learning; Equilibrium optimizer; Medical image segmentation; Image classification.

INTRODUCTION

Brain tumors (BT), are one of the primary types of cancer that drive up the mortality rates of people all over the world [1]. There has been a dramatic increase in the global incidence of brain tumors. Death from brain tumors is relatively common, taking the lives of thousands annually. Glioma, the common primary BT, occurs because of the carcinogenesis of glial cells in the brain. Glioma can be characterized by various malignancies and histological grades, with an average survival duration of less than fourteen months after analysis for glioblastoma patients [2]. A renowned non-invasive method that generates large and different tissue contrasts in every imaging modality is magnetic resonance imaging (MRI), and it is broadly employed by healthcare specialists for diagnosing BT [3]. But the manual analysis and segmentation of structural MRI images of BT was a hard and time-consuming task that was executed by experienced neuroradiologists. Hence, robust and automatic BT segmentation has a great effect on BT treatment and diagnosis [4].

Automatic classification and segmentation of medical images have made a great contribution to the treatment, diagnostics, and growth prediction of BTs [5]. An initial BT diagnosis has a faster response to treatment, which enhances the survival rate of patients. Classification and location of BTs in large medical image databases, considered routine clinical tasks by manual processes, have a higher cost both in time and effort [6]. A classification process, automatic detection, and location were worthwhile and desirable. Conventional ML-related techniques, like Random Forest (RF), Support Vector Machines (SVM), and the k-nearest neighbours algorithm KNN, can usually be used for BT analysis. But such techniques have the common restriction of extracting features through hand-craft in the modelling stage [7].

Deep learning (DL)-related techniques solve the disadvantage of feature extraction through handcraft. DL has enabled the development of massively scalable trainable techniques capable of acquiring the optimal properties for a specific context. DL can be powerful and displays traditional ML in numerous domains, such as medical image segmentation, computer vision (CV), and speech recognition. DL has a deep neural network framework with numerous layers [8]. With the advancement of DL and relevant technologies, the technique related to DL is becoming the mainstream technique in the domain of CV. Recently, convolutional neural networks (CNN) were leveraged in retinal segmentation tasks, and outstanding segmentation outcomes were continually achieved [9]. The authors have also integrated Fully Convolutional Networks (FCN) and CNN to scale up the segmentation outcome after deriving the U-Net method via FCN. Several writers have modelled several improved techniques on its lesser amount of data for training an end-wise network, like DRNet, R2U-Net, CURU, and S-U-Net [10].

With this study, a new algorithm for brain MRI tumor classification and segmentation using an equilibrium optimizer and deep learning (EOADL-BTSC) is presented. In the first stage of the presented EOADL-BTSC method, contrast enhancement and skull stripping are performed as preprocessing. For medical image segmentation, we design an EOA using an attention-inception-based UNet approach. In addition, the capsule network model is utilised to extract features. Finally, BT classification was accomplished with the help of a cascaded recurrent neural network (CRNN). The MRI data set is used to verify the validity of the new approach and ensure it can withstand experimental inspection.

RELATED WORK

Raza and coauthors devised a hybrid DL technique named DeepTumorNet for three kinds of BTs pituitary tumor classification, glioma, and meningioma by implementing a fundamental CNN architecture [11]. The GoogLeNet CNN architecture method has been employed as a foundation. While advancing the hybrid

DeepTumorNet method, the final five layers of GoogLeNet have been eliminated, and fifteen novel layers are included instead of those five. Yin B and coauthors proposed an innovative metaheuristic-related technique offered for early diagnosis of BT to prevent this objection [12]. This devised technique involves three main stages, which include classification, background removal, and feature extraction related to MLP-NN. Therefore, an enhanced version of the WOA technique related to chaos theory and the logistic mapping method was used for optimal feature selection and the classification phases.

Anaraki AK and coauthors came up with a technique related to CNN and GA was modelled to noninvasively categorise various grades of glioma utilising MRI [13]. The presented method utilises GA to evolve the CNN structure, as opposed to the standard practice of employing either trial-and-error or predetermined common structures when selecting a DNN architecture. Kumar and coauthors modelled an optimized DL system called Dolphin-SCA-related Deep CNN for enhancing accuracy and making effective decisions in categorization [14]. The segmentation procedure can be executed through a fuzzy deformable fusion method with dolphin echolocation-related SCA (Dolphin-SCA). The derived features were employed in the deep CNN to execute the BT classification with Dolphin-SCA as the training algorithm. Hu A and coauthors proposed an innovative metaheuristic-related system was modelled for initial recognition of BTs. The presented technique applies three key steps called classification, tumor segmentation, and feature extraction related to a DBN. An enhanced version of the seagull optimization method was implemented for selecting the features optimally and classifying the images [15].

Deb and coauthors devised and modelled a new segmentation and classification method for BT detection [16]. The devised system employs adaptive fuzzy DNN with frog leap optimization for identifying abnormalities and normalities in images. After that, the abnormal image was segmented by utilising the adaptive flying squirrel method, and the tumor size was identified, which was employed for finding the tumor severity. Raju and coauthors devised the automatic technique of classification utilising the Harmony Crow Search (HCS) optimised method for training multi-SVNN methods [17]. The Brain Tumor detection was executed through the Bayesian fuzzy cluster technique, and tumor categorization was done through the presented HCS optimization method-related multi-SVNN technique. The degree to which the features of the segments generated by Bayesian fuzzy clustering are utilised, as determined by the devised strategy to classification, is known as the BT. Table 1, a look at how various approaches stack up.

Table 1. Comparison of state-of-art methods

S.NO	AUTHOR	YEAR	PROPOSED METHOD	ACCURACY ACHIEVED	LIMITATIONS
1.	Raza A et al.	2022	DeepTumorNet (The foundation was laid with GoogLeNet architecture).	99.67%	High computational requirements, Gradient vanishing/exploding
2.	Yin B et al.	2020	whale optimization algorithm (Based on Chaos theory).	87%	Sensitivity to parameter tuning, Lack of convergence guarantees.
3.	Anaraki AK et al.	2019	CNN and Genetic algorithms.	94.2%	Slow convergence, Inefficiency in handling constraints.
4.	Kumar S et al.	2020	Dolphin-SCA based Deep CNN.	96.3%	Lack of interpretability, Lack of spatial invariance.
5.	Hu A et al.	2021	Improved Seagull Optimization Algorithm (ISOA).	88%	Computationally complex, Limited scalability.
6.	Deb D et al.	2021	Adaptive Fuzzy Deep Neural Network (AFDNN) with frog leap optimization.	99.6%	Lack of parallelization efficiency, Lack of robustness.
7.	Raju AR et al.	2018	Harmony-Crow Search (HCS)-based multi-Support Vector Neural Network (SVNN).	93%	Complexity and interpretability, Sensitivity to feature scaling

THE PROPOSED MODEL

As part of this study, a novel EOADL-BTSC approach was formulated for BT segmentation and classification on brain MRI. The presented EOADL-BTSC technique involves different phases of operations such as pre-processing, attention inception-based UNet segmentation, EOA-based parameter tuning,

capsule network feature extraction [18], and CRNN classification. Images are adjusted for better contrast before skull stripping is done. Next, the segmentation of MRI is performed by EOA with an attention-inception-based UNet model. Finally, the capsule network feature extraction and CRNN classification processes are carried out.

EOADL-BTSC, EOA, Capsule network model, and CRNN are technical terms and acronyms used in the article to describe the proposed methodology for brain tumor segmentation and classification using MRI images. EOADL-BTSC stands for Equilibrium Optimizer Algorithm with Deep Learning-based Brain Tumor Segmentation and Classification. This is the name of the proposed method that combines various deep learning algorithms and techniques for automated brain tumor segmentation and classification. EOA refers to the Equilibrium Optimizer Algorithm, which is used to optimize the hyperparameters of the attention-inception-based UNet model. Capsule network model is a type of neural network (NN) architecture that is used for feature extraction in the proposed method. CRNN, which is used for the classification process in the proposed method. Figure 1 depicts the schematic diagram of the EOADL-BTSC approach.

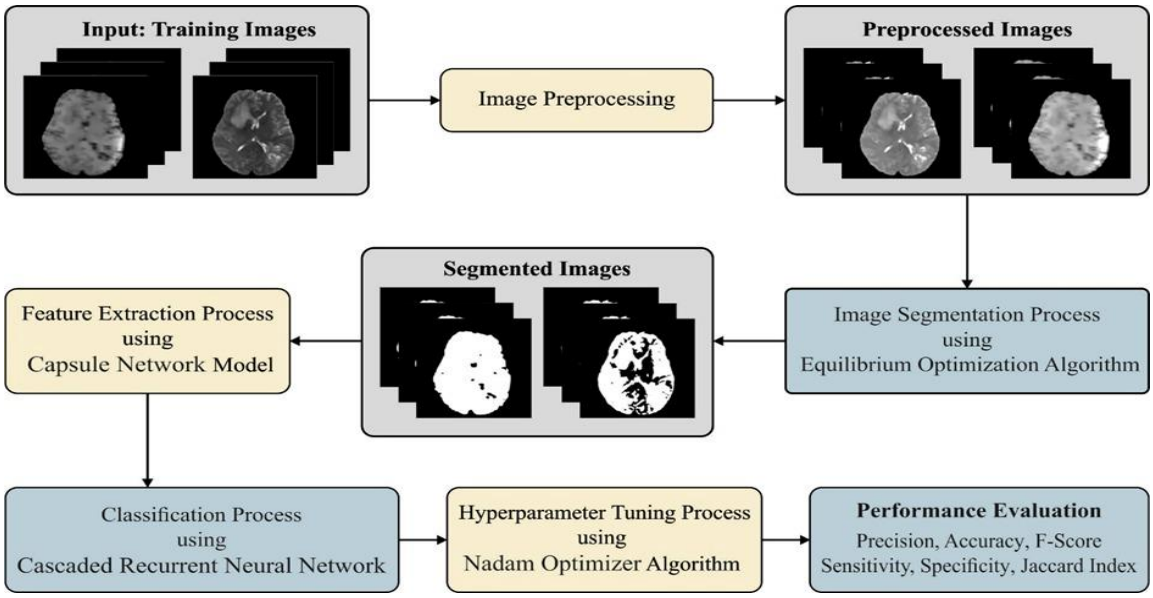

Figure 1. Schematic diagram of EOADL-BTSC system

The proposed methodology comprises several stages, each of which performs a specific function in the segmentation and classification of brain tumors in MRI images. To begin, the input MRI images undergo preprocessing with enhancement of contrast and skull stripping methods to boost contrast and eliminate non-brain tissues, respectively. Then, the preprocessed images are fed into the EOA with an attention-inception-based UNet model, which performs the task of segmentation by generating a pixel-wise mask indicating the regions of the brain affected by tumors. After tumor regions have been segmented, the CapsNet model is used to extract features that are clinically relevant to the tumor. Finally, the extracted features are fed into the CRNN model, which performs the task of classification by assigning proper class labels to the MRI images, indicating the type and severity of the tumor. The block diagram also shows the hyperparameter tuning stage using the EOA, which selects the optimal hyperparameters for the attention-inception-based U-Net model. Overall, the EOADL-BTSC approach provides an end-to-end solution for accurate and fast segmentation and classification of brain tumors in MRI images.

Image Pre-processing

The image pre-processing takes place in two ways: CLAHE (Contrast-Limited Adaptive Histogram Equalization) - based enhancement of contrast and skull stripping. CLAHE works on smaller regions of images, termed tiles, instead of the complete image [19]. The surrounding tiles were blended using bilinear interpolation to remove the false boundary. This technique was utilised to improve image contrast. Skull stripping is the extraction of unwanted elements and non-brain anatomy from scanned images. The down-sampling strategy utilises five convolutional blocks. Presently, there are 1024 feature maps. But the final block, max pooling with stride 2, is carried out after the completion of all the blocks for down-sampling. The feature map has decreased in size from 240×240 to 15×15. All the up-sampling blocks initiate with a deconvolution layer of stride 2 and filters of size 3×3. Therefore, feature map was developing gradually

popular. The two convolutional layers in the up-sampling block lessen the deconvolution feature map quantity and feature map in the encoder route.

Image Segmentation

At this stage, the segmentation of MRI is performed by EOA with an attention-inception-based UNet model [20]. During the encoder stage, a novel image X is primarily processed with a 3×3 convolutional layer with ReLU and BN functions for obtaining a feature map (FM) in the primary encoder step, where $e\_out(0)$ signifies the primary encoding path outcomes. During the succeeding 2nd and 3rd layers, 2 residuals, one inception, and $scSE$ elements were utilised for extracting and refining features. It can be developed two kinds of residual elements that utilise dilated convolutional with rates of dilation of 2 and 3, respectively. The above encoder process, where $\mathrm{Res}\_dilation(f,n)$ represents the conduct residual elements with convolutional whose dilation is n on FM f.

During the decoder step, primarily, the resolution of the heatmap attained in the encoder part was improved with the presented dynamic upsampling-transpose convolutional process; afterward, the outcome was a skipped connection with equivalent FM in the encoder step; as a result, there are now 112 (64+48) image channels. The skip connection formula, where $de\_out(i-1)$ defines the result of the $(i-1)^{th}$ decoding step and $e_{out}(n-i-1)$ represents the outcome of the equivalent $(n-i-1)^{th}$ encoding stage. The presented dynamic transpose and upsampling process for amplifying FM twice. Afterward, with a residual element with rate of dilation of 2 is implemented, and the feature weight is altered with the $scSE$ element. $de\text{-}in(i)$ signifies the i^{th} input of the decoding stage. The secondary decoding stage was applied in like manner, and then the secondary dynamic upsampling-transpose and skip connection stage developed a count of 88 $(56+32)$ channels, and feature weighting was changed over with residual dilation and $scSE$ elements. A multiple scales feature amalgamation strategy is employed, which combines the results from each decoder stage to improve segmentation accuracy, especially for thin vessel segmentation. The sigmoid function was used to generate the segmentation results map after a conv 3×3 layer having stride 1 was applied to the combined feature from various decoder stages.

A multiscale extraction of features and representation improvement method, it can establish the inception process in the encoder step, improve the attention system dependent upon the $scSE$ element, and then inception element in both the encoder and decoder steps. Afterward all the phases of the decoder stage, it can obtain distinct resolution side outcomes that comprise various scale data, contributing to improving segmentation quality. Noticeably, it adds convolutional 1×1 afterwards scSE element and utilises the equivalent times upsampling function for making the decoding stage features for restoring a novel image resolution. Then, the channel-level multi-feature obtained can be merged into a single one. The entire procedure was defined as Equations. (1) and (2).

$$s_j = up\big(conv\big(de\_out(i)\big), 2^{n-i-1}\big), i = 0,1,\dots,n-1 \qquad (1)$$

$$f = concat[s_0, s_1, .., s_{n-1}] \qquad (2)$$

Whereas n represents the height of our network, $de\_our(i)$ has present decoding stage outcomes, $conv$ denotes the convolutional with kernel size 1×1, and up indicates the upsampling function with scale factor $2^{n-i-1}s$ which implies the i^{th} multi-scale feature side outcome. It is created in concatenation with Equation (2) for correlating every multi-level feature for realising feature fusion and obtaining the last fusion outcome f. At last, it can be utilised convolutionally 3×3 to achieve the last segmentation outcome.

The EOA is used to adjust the hyperparameters of the segmentation component. The EOA is a recently created metaheuristic strategy that uses a balanced pool and candidate to upgrade particles, and it is related to physics in order to deal with ongoing optimisation difficulties [21].

In this methodology, the authors used an Equilibrium Optimization Algorithm (EOA) to tune the hyperparameters of the attention-inception-based UNet method for medical image segmentation. The EOA is a type of metaheuristic optimization algorithm that is designed to efficiently tune the hyperparameters of machine learning models. The following hyperparameters of the attention-inception-based UNet method were tuned using the EOA:

Number of filters: To boost segmentation accuracy, the UNet model's number of filters per convolutional layer was fine-tuned.

Dropout rate: The dropout rate is a regularization technique that helps in preventing overfitting of the model. The EOA was used to tune the dropout rate to achieve better segmentation results.

Learning rate: When training an optimisation algorithm, the learning rate is a critical hyperparameter because it determines the size of the training steps. To improve segmentation outcomes, the EOA was utilised to fine-tune the UNet model's learning rate.

Batch size: When training a neural network, the batch size determines how many samples are sent into the network at once. Better segmentation outcomes were achieved by tuning the batch size of the UNet model using the EOA.

The EOA was used to tune these hyperparameters of the attention-inception-based UNet method in an automated and efficient manner. By tuning these hyperparameters, the EOA helped in improving the accuracy and performance of the proposed EOADL-BTSC approach for segmenting and classifying the brain tumor.

The EOA has improved capabilities for both exploration and exploitation, and it also reduces the likelihood of becoming stuck in a local optimum. The mass balance is analytically resolved as follows:

$$C = C_{eq} + \left(C_0 + C_{eq}\right).F + \frac{G}{\lambda V}(1 - F), \qquad (3)$$

In Equation (3), V is regarded as being 1 as a volume unit.

An equilibrium pool of four viable candidates plus a fifth averaged one, is generated by the EOA.

$$C_{eqs,poo1} = \left\{C_{eqs(0)}, C_{eqs(1)}, C_{eqs(2)}, C_{eqs(3)}, C_{ave}\right\}, \qquad (4)$$

$$C_{ave} = \frac{C_{eqs(0)} + C_{eqs(1)} + C_{eqs(2)} + C_{eqs(3)}}{4}. \qquad (5)$$

The candidate's fitness in a balanced pool must satisfy the following rules for the given problem, expressed as f.

$$f\left(C_{eqs(0)}\right) \le f\left(C_{eqs(1)}\right) \le f\left(C_{eqs(2)}\right) \le f\left(C_{eqs(3)}\right). \qquad (6)$$

EOA employs the iterating and initializing approaches as other bioinspired techniques while resolving problems, whether they come from real engineering work or are specified as benchmarks. The EOA's methods of discovery and development are ongoing iterations. To enhance effectiveness, there were many processes involved in building the EOA.

The problem at hand may be assumed to be bounded by symmetric or asymmetric domains with [lb, ub], and the candidate swarm is distributed uniformly. To accomplish this, a pseudo-random number r_1 is presented:

$$C_i = lb + (ub - lb).r_1. \qquad (7)$$

The location vector for $i\text{-}th$ candidate is C_i, the position of the candidate for the subsequent iteration is substantial in three stages. C_{eq} represent a randomly chosen candidate from the pool. There is an F exponential parameter that is defined by:

$$F = a_1 sign\,(r_2 - 0.5)(e^{-\lambda t} - 1), \qquad (8)$$

Whereas a_1 denotes a fixed parameter that governs exploration and the ability to partition exploration and exploitation into sub-processes, respectively. The high value of a_1 indicates a high probability for the candidate to perform exploration and a small probability for the candidate to perform exploitation. For convenience and experience, $a_1 = 2.r_2$ denotes another random value within $[0,1]$, and t indicates a variable expressed to be associated with the iteration times.

$$t = (1 - \frac{iter}{\max Iter})^{\left(\frac{a_2 iter}{\max Iter}\right)}, \qquad (9)$$

In Equation (9), $iter$ indicates the present iteration number, and $MaxIter$ indicate the maximal iteration number. Here, G denotes the parameter for the candidate's rate of generation that improves their exploitability:

$$G = G_o F, \qquad (10)$$

$$G_o = GCP\left(C_{eq} - \lambda C\right), \qquad (11)$$

$$GCP = \begin{cases} 0.5, & r_2 \ge GP, \\ 0, & r_2 \ge GP, \end{cases} \qquad (12)$$

GP denotes generation probability. GP was fixed at 0.5 to accomplish the best outcomes in balancing probability among exploration and exploitation:

$$C = C_{eq} + \left(C - C_{eq}\right).F + \frac{G}{\lambda V}(1 - F), \qquad (13)$$

In Equation (13), F is described in Equation (8), and V is regarded as a unit.

CapsNet Model-Based Feature Extraction

In this study, we used the CapsNet model to generate feature vectors. Hinton created a new type of Neural Network called the capsule network. The fundamental architecture encompasses the digital capsule, input, convolution, output, and primary capsule layers [22]. During the convolutional layer, the convolutional layer of CNN can be exploited for extracting low-level features. The convolutional kernel was employed for more feature extraction to acquire numerous capsules. The CapsNet framework is used for the extraction of features in the proposed system for segmenting and classifying brain tumors using the EOADL-BTSC approach. The CapsNet model is a type of NN architecture that is designed to model spatial relationships between objects in an image. The CapsNet model is used for extracting features in the proposed system because it is particularly effective at capturing the spatial relationships between different structures in medical images. This can be helpful in identifying the boundaries of brain tumors and accurately segmenting them from surrounding healthy tissue. To verify the effectiveness of the capsule network model for feature extraction in the proposed system, the researchers carried out a series of simulation analyses using a benchmark database. The experimental validation showed that the proposed EOADL-BTSC method outperformed several other recent approaches in terms of several performance measures, including segmentation accuracy and dice similarity coefficient. Therefore, based on the experimental results and the theoretical understanding of the capsule network model, it can be justified that the use of a capsule network model for extraction of features is an effective approach in the proposed system for segmenting and classifying brain tumor using the EOADL-BTSC method.

In comparison to CNN, CapsNet exploits vector capsules for replacing neurons, dynamic routing for replacing the squash function, and pooling operations for replacing the ReLu activation function. u_i characterises the output of $i\text{-}th$ low-level capsules, $W_{i|j}$ signifies weight matrices among i and j low- and high-level capsules, and $\hat{\mathrm{u}}$ signifies the predicted output of j low-level capsules :

$$\hat{u} = W_{i|j}u_i. \qquad (14)$$

Where S_j and V_j refer to the input and output of high-level capsules:

$$S_j = \sum_i C_{ij}\,\hat{u}_{i|j}. \qquad (15)$$

Where C_{ij} represents the expected vector's coupling coefficient $\hat{u}_{i|j}$ of low-level capsules. CapsNet uses activity vectors to describe the existence and properties of entities. Different qualities are initially represented by vector values of different dimensions, and then the vector mod is used to characterise the entity's occurrence probability. The vector was normalized and compressed using a non-linear calculation to provide occurrence probability of elements between 0 and 1:

$$V_j = \frac{\|s_j\|^2}{1 + \|S_j\|}\frac{S_j}{\|s_j\|}. \qquad (16)$$

In Equation (16), The CapsNet output vector is denoted by V_j.

C_{ij} represents the coupling coefficient that is defined by the dynamic routing iteration model. If $C_{ij} = 0$, it shows that there is no data transmission amongst i and j low- and high-level capsules:

$$C_{ij} = \frac{\exp\,(b_{ij})}{\sum_k \exp\,(b_{ik})}. \qquad (17)$$

Whereas b_{ij} signifies the logarithmic probability of coupling among capsules i and j that can be initialised to 0:

$$b_{ij} + \hat{u}_{j|i} \cdot V_j \rightarrow b_{ij}. \qquad (18)$$

CapsNet uses a high-level capsule's vector length to represent the probabilities associated with a category, allowing the approach to select the class of a higher-level capsule with the longest possible output vector as a category to predict.

$$L_j = T_j \max(0, m^+ - \|V_j\|)^2 + \lambda(1 - T_j) \max(0, \|V_j\| - m^-)^2. \quad (19)$$

In Equation (19), T_j designates whether $j\text{-}th$ class exists; m^+, m^- and λ denote superparameter that should be stated before.

Pseudocode of proposed method is given below.

```
Input: MRI images with brain tumors
Output: Segmented brain tumors with classification labels

// Preprocessing
Enhance image contrast
Strip skull from image

// Segmentation
Initialize UNet model with attention-inception blocks
Use EOA to optimize UNet hyperparameters
Train UNet on MRI images with segmented brain tumors

// Feature Extraction
Initialize Capsule Network model
Use trained UNet to extract features from segmented tumor regions
Train Capsule Network on extracted features

// Classification
Initialize CRNN model
Use trained Capsule Network to classify tumor regions
Assign proper classification labels to tumor regions
```

Image Classification using CRNN Model

For effective BT classification, the CRNN model is used to allot appropriate class labels. Recurrent Neural Network (RNN) is a branch of Artificial Neural Network (ANN) that is an augmented edition of conventional Feed Forward Neural Network (FFNN) with connections and loops [23]. Different from FFNN, the RNN can evaluate input sequences by means of recurrent hidden states with activation of the preceding step. Thus, the system represents a temporal behaviour that is always changing. Assuming the sequential dataset $(x_1, x_2, \ldots, x_T)$, where x_i indicates the dataset in the i^{th} time step, RNN upgrades the recurrent hidden state h_t as follows:

$$h_t = \begin{cases} 0, & if\, t = 0 \\ \phi(h_{t-1}, x_t), & otherwise \end{cases} \quad (20)$$

In Equation (20), ϕ shows a nonlinear function. Consequently, RNN includes output $(y_1, y_2, \ldots, y_T)$. Ultimately, data classification was executed by output y_T. The RNN method's recurrent concealed state update rule is expressed as follows:

$$h_t = \phi(W x_t + U h_{t-1}) \quad (21)$$

In contrast, W and U represent the recurrent hidden unit's input and activation coefficient matrices, respectively.

$$p(x_1, x_2, \ldots, x_T) = p(x_1) \cdots p(x_T | x_1, \ldots, x_{T-1}). \quad (22)$$

Then, the conditional probability distribution can be presented as follows:

$$p(x_t | x_1, \ldots, x_{t-1}) = \phi(h_t) \quad (23)$$

Where h_t is acquired from (20) and (23). The hyperspectral pixel can be processed as a sequence dataset, and a recurrent network was employed to model the spectral sequence. Figure 2 depicts the architecture of CRNN. RNN performs better in ML and computer vision tasks because of the importance of the DL model. An advanced recurrent unit is added to solve this issue. Long short-term memory (LSTM) is a type of recurrent concealed units well-suited to learning lengthy sequences of data. The CRNN architecture is a type of deep neural network that combines the capabilities of CNNs and RNNs. The CRNN architecture is designed to process sequential data, such as time-series or sequences of images. The CRNN architecture consists of three main components: a CNN layer, an RNN layer, and a fully connected layer. The CNN layer is responsible for feature extraction from the input data. The RNN layer then takes over to record the features' temporal dependencies. The layer that is completely connected is then deployed during classification or regression operations. In the context of the proposed EOADL-BTSC approach, the CRNN is used for classification of brain tumor images into their respective classes. The CRNN takes as input the features extracted by the Capsule Network model and the temporal dependencies between these features are captured by the RNN layer. A probability distribution over the types of brain tumors is what the CRNN produces as an output.

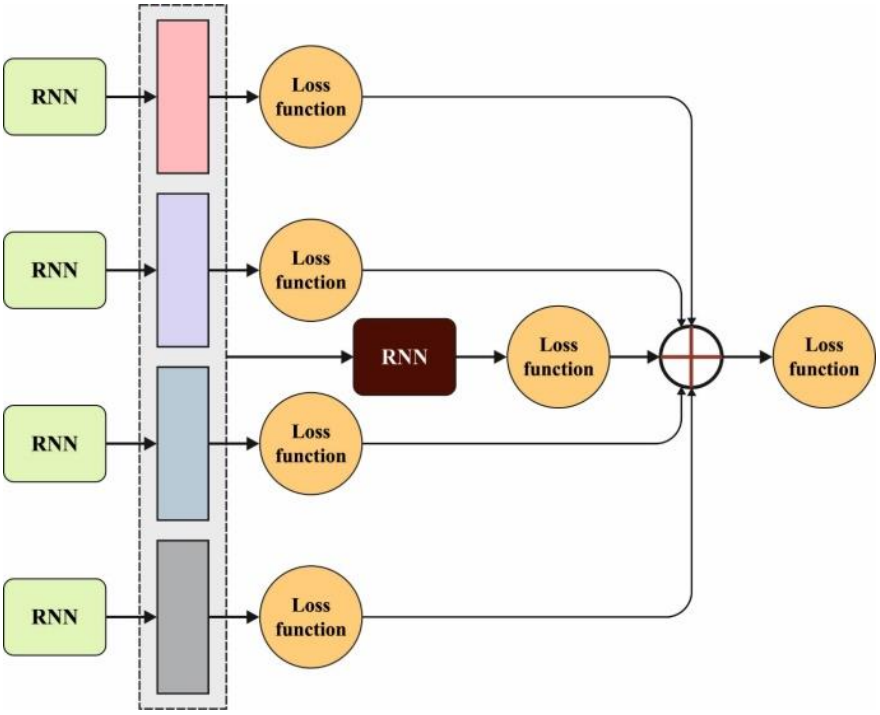

Figure 2. Structure of CRNN

In comparison to the LSTM units, With Gated Recurrent Unit (GRU), only need a limited number of training cases and the variables you do need for classification have to be kept to a minimum. GRU is a type of RNN layer that is often used in the CRNN architecture. The CRNN architecture combines CNNs and RNNs to learn features from variable-length sequential data. In order to determine specific characteristics of the input sequence, the CNN layers are employed, while the RNN layers are used to model the temporal dependencies in the sequence. The GRU layer is used in the RNN part of the CRNN architecture to capture long-term dependencies in the sequence. It is a variant of the traditional RNN layer that uses gating mechanisms to selectively update and forget information from the previous time step. This makes it more effective in dealing with vanishing gradients, which can be a problem in traditional RNNs when learning long-term dependencies. In general, the GRU layer in the CRNN architecture is crucial for accurately modelling the input sequence's temporal dynamics.

Consequently, GRU can be chosen as a building block for RNN. The two-gate unit used by GRU to regulate data flow was a crucial component of the system.

$$h_t = (1 - u_t)h_{t-1} + u_t\tilde{h}_t \quad (24)$$

In Equation (24), u_t designates the update gate that is given as follows:

$$u_t = \sigma(w_u x_t + v_u h_{t-1}) \quad (25)$$

In Equation (25), σ depicts a sigmoid function, w_u denotes a weight value, and v_u means the weight vector.

$$\tilde{h}_t = tanh\big(wx_t + V(r_t \odot h_{t-1})\big) \quad (26)$$

In Equation (26), $\odot$ refers to component-wise multiplication, and r_t means the reset gate as

$$r_t = \sigma(w_r x_t + V_r h_{t-1}) \quad (27)$$

Specifically, the data series x is categorised into l subsequence $z = (z_1, z_2, \cdots, z_l)$, where it encompasses different class labels. Then, for the last subsequence z_l, the length of alternative subsequences is $d = floor(k/l)$, which represents the closest integer less than or equal to k/l.

$$z_i = \begin{cases} (x_{(i-1)\times d+1}, \cdots, x_{i\times d}), & if i \neq l, \\ (x_{(i-1)\times d+1}, \cdots, x_k), & otherwise. \end{cases} \quad (28)$$

Furthermore, every subsequence is fed into the first layer of RNN, which contains an analogous structure and distributes parameters to decrease parameters. In the case of subsequence $\mathrm{z_i}$, each sample can be made up of outcomes from GRU. The last feature representation for $\mathrm{z_i}$ is denoted as $\mathrm{F_i^{(1)}} \in \Re^{\mathrm{H_1}}$, whereby $\mathrm{H_1}$ indicates the hidden layer size in the initial layer RNN. Later, $\mathrm{F_i^{(1)}}, \mathrm{i} \in \{1,2,\cdots,\mathrm{l}\}$ was integrated to generate sequence $\mathrm{F} = (\mathrm{F_1^{(1)}}, \mathrm{F_2^{(1)}}, \cdots, \mathrm{F_l^{(1)}})$, whose length was l. This sequence was induced into the next layer of RNN for learning additional detail. Similarly, the initial layer RNN employs the resultant of GRU as learned feature $\mathrm{F^{(2)}}$. The classification outcomes of x are acquired by inducing input $\mathrm{F^{(2)}}$ into the resulting layer with equal-sized candidate classes C.

The proposed EOADL-BTSC method involves a series of deep learning models and algorithms working together to segment and classify brain tumors in MRI images. Here, we can provide a mathematical example of the Equilibrium Optimization Algorithm (EOA) used in this method:

The EOA is used to tune the hyperparameters of the attention-inception-based U-Net model used for segmenting medical images. The EOA works by iteratively adjusting the hyperparameters until the best possible values are obtained. The EOA involves three main steps:

Step 1: Initialization of parameters

Initialize the search space X, which contains the hyperparameters to be optimized. For example, if we have three hyperparameters, the search space X can be defined as X = [x1, x2, x3]. Set the initial guess x0 in the search space, which is the starting point for the optimization process.

Step 2: Equilibrium optimization process

The EOA algorithm then performs the following steps in each iteration:

Select the equilibrium point xeq: This is done by randomly selecting a point in the search space X.

Perturb the equilibrium point: A small perturbation is added to the equilibrium point to create a new point in the search space. This new point is denoted as xpert.

Evaluate the objective function at the equilibrium point and perturbed point: The objective function is evaluated at both the equilibrium point xeq and perturbed point xpert. The objective function measures how well the U-Net model is performing on the MRI images.

Determine the new equilibrium point: The evaluations of the objective functions are used to establish a new equilibrium point. If the perturbed point xpert yields better results than the equilibrium point xeq, then xpert becomes the new equilibrium point. Otherwise, xeq remains the equilibrium point.

Update the search space: The search space is updated by moving the equilibrium point xeq towards the new equilibrium point.

Until a stopping requirement is satisfied, such as a maximum number of iterations or a minimum improvement level, the EOA algorithm repeats these steps.

EVALUATION METRICS

When compared to conventional approaches, the proposed strategy is shown to yield superior results. The proposed work was evaluated by applying it to sample images and calculating its Accuracy, PPV, Sensitivity, Specificity, F-Score, and Jaccard Index.

The accuracy of the model is the most fundamental indicator of its predictive power. It's a measure of how often a prediction turns out to be right. Below, in Equation 29, is the mathematical definition of accuracy.

$$\boldsymbol{Acc = \frac{TP + TN}{TP + FP + TN + FN}} \qquad (\mathbf{29})$$

Precision also known to as positive predicted value (PPV) is the rate at which correct predictions are made relative to the entire number of correct forecasts. The accuracy of the model's positive predictions is evaluated, and its capacity to suppress false positives is gauged. The mathematical representation PPV is defined in Equation 30:

$$\boldsymbol{PPV(S_1, S_2) = \frac{|S_1 \cap S_2|}{|S_2|}} \qquad (\mathbf{30})$$

When evaluating a model's performance on a classification task, sensitivity indicates how many positive examples the model gets right out of a total of all possible positive examples. Equation 31 defines is the mathematical expression for it.

$$\boldsymbol{Sensitivity = \frac{TP}{TP + FN}} \qquad (\mathbf{31})$$

The level of specificity quantifies how many times false negative predictions were made relative to the total number of false negatives. Accuracy in avoiding false negatives is a supplementary measure to recall. Equation 32 defines specificity mathematically.

$$\boldsymbol{Specificity = \frac{TN}{TN + FP}} \qquad (\mathbf{32})$$

The Jaccard index is the ratio of the regions that overlap in both the prediction and the ground truth to the union of the two. The overlap between the anticipated and ground-truth zones or masks is a measure of how closely they match. Its mathematical form is represented in Equation 33:

$$\boldsymbol{Jac = \frac{|S_1 \cap S_2|}{|S_1 \cup S_2|}} \qquad (\mathbf{33})$$

EXPERIMENTAL VALIDATION

This section examines the step by step experimental steps with its real outputs. Collect a dataset of MRI images with brain tumors. The dataset should be diverse and representative of different types of brain tumors and imaging conditions. Preprocess the MRI images to enhance the contrast and remove any non-brain tissue such as skull and background noise. Use the EOADL-BTSC method to segment the brain tumors in the preprocessed images. This involves initializing the UNet model with attention-inception blocks, optimizing the hyperparameters using EOA, training the UNet model on the preprocessed MRI images with segmented brain tumors, and obtaining the segmented brain tumors. Use the trained UNet model to extract features from the segmented tumor regions, and feed these features to the CapsNet model. Train the CapsNet model on the extracted features. Use the trained CapsNet model to classify the tumor regions into different types of brain tumors using the CRNN model. Assign proper classification labels to the tumor regions. Evaluate the performance of the proposed EOADL-BTSC method on a separate testing dataset using appropriate evaluation metrics such as accuracy, sensitivity, specificity, and F1 score. Evaluate the suggested EOADL-BTSC approach against other top-tier brain tumor segmentation and classification techniques. Report the experimental results in the form of tables, graphs, and figures, along with a detailed analysis and interpretation of the results.

In this part, we look at how well the EOADL-BTSC approach performs on the BraTS 2019 dataset and the BraTS 2020 dataset when it comes to BT categorization. In Figure 3, we see a selection of sample MRIs.

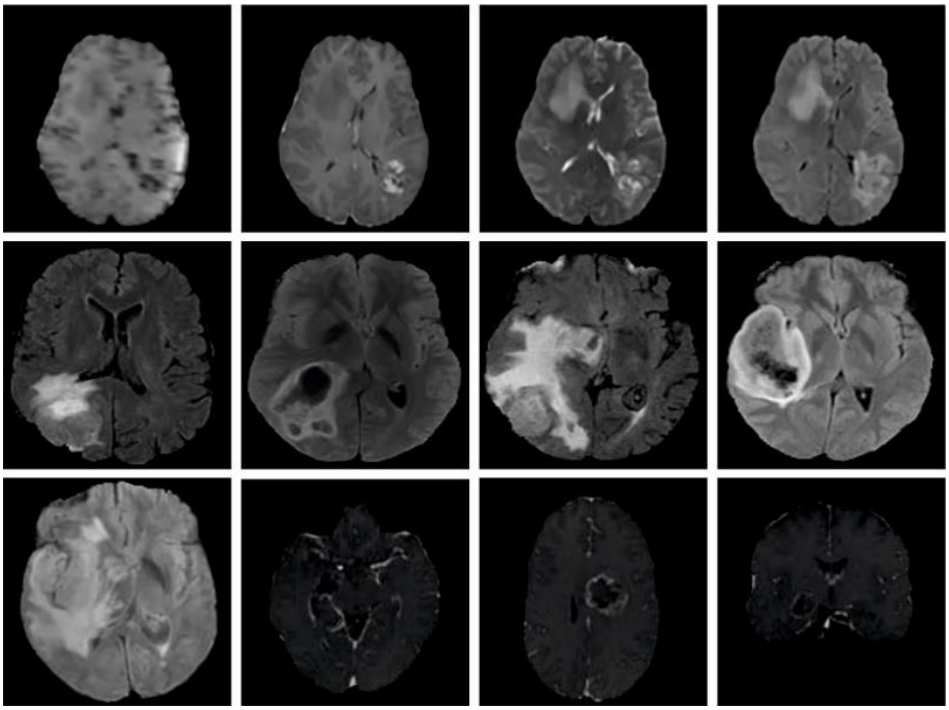

Figure 3. Sample images

The confusion matrices created by the EOADL-BTSC technique on the BraTS 2019 database are revealed in Figure 4. The results showcased that the EOADL-BTSC method has properly identified the normal and abnormal BT classes.

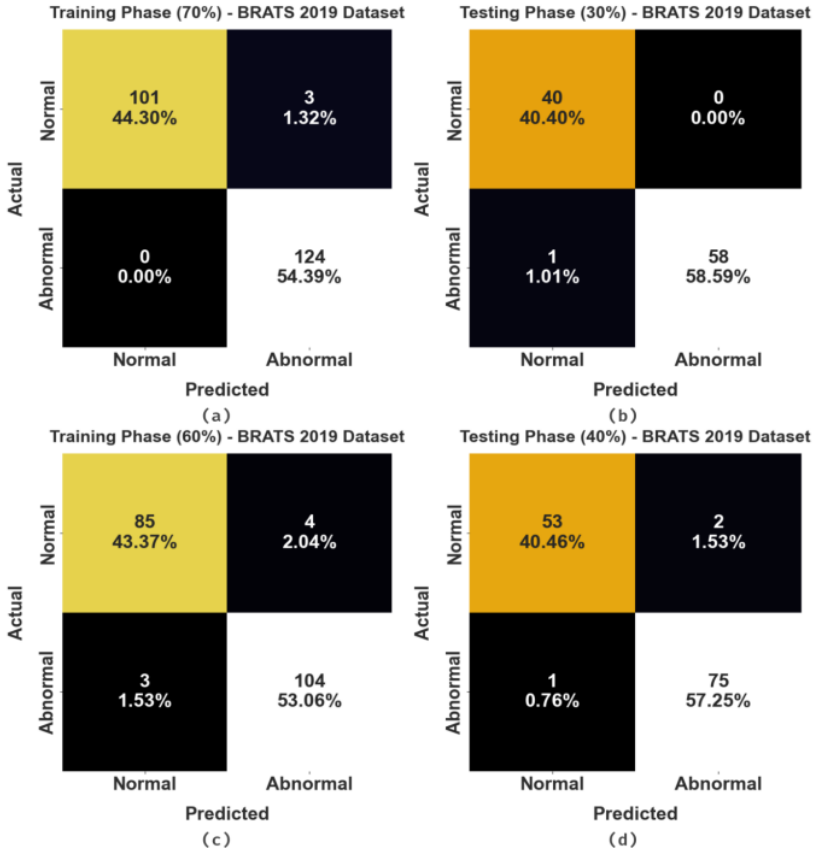

Figure 4. Confusion matrices of EOADL-BTSC system BraTS 2019 dataset (a-b) TR and TS databases of 70:30 and (c-d) TR and TS databases of 60:40.

Table 2 offers detailed BT classification results for the EOADL-BTSC model on the BraTS 2019 dataset. The results implied the improved efficacy of the EOADL-BTSC model in all classes. For the sample, on 70%

of the TR database, the EOADL-BTSC methodology has attained an average $accu_{bal}$ of 98.56%, PPV of 98.82%, $sens_y$ of 98.56%, $spec_y$ of 98.56%, F_{score} of 98.67%, and JI of 97.38%. Meanwhile, on 30% of the TS database, the EOADL-BTSC method has obtained an average $accu_{bal}$ of 99.15%, PPV of 98.78%, $sens_y$ of 99.15%, $spec_y$ of 99.15%, F_{score} of 98.96%, and JI of 97.93%. Eventually, on 60% of the TR database, the EOADL-BTSC method has achieved an average $accu_{bal}$ of 96.35%, PPV of 96.44%, $sens_y$ of 96.35%, $spec_y$ of 96.35%, F_{score} of 96.39%, and JI of 93.04%.

Table 2. BT classification outcome of EOADL-BTSC system with various measures under BraTS 2019 dataset

BraTS 2019 Dataset						
Class	**Accuracy$_{bal}$**	**PPV**	**Sensitivity**	**Specificity**	**F-Score**	**Jaccard Index**
Training Phase (70%)						
Normal	97.12	100.00	97.12	100.00	98.54	97.12
Abnormal	100.00	97.64	100.00	97.12	98.80	97.64
Average	**98.56**	**98.82**	**98.56**	**98.56**	**98.67**	**97.38**
Testing Phase (30%)						
Normal	100.00	97.56	100.00	98.31	98.77	97.56
Abnormal	98.31	100.00	98.31	100.00	99.15	98.31
Average	**99.15**	**98.78**	**99.15**	**99.15**	**98.96**	**97.93**
Training Phase (60%)						
Normal	95.51	96.59	95.51	97.20	96.05	92.39
Abnormal	97.20	96.30	97.20	95.51	96.74	93.69
Average	**96.35**	**96.44**	**96.35**	**96.35**	**96.39**	**93.04**
Testing Phase (40%)						
Normal	96.36	98.15	96.36	98.68	97.25	94.64
Abnormal	98.68	97.40	98.68	96.36	98.04	96.15
Average	**97.52**	**97.78**	**97.52**	**97.52**	**97.64**	**95.40**

Table 3. BT classification outcome of EOADL-BTSC system with various measures under BraTS 2020 dataset

BraTS 2020 Dataset						
Class	**Accuracy$_{bal}$**	**PPV**	**Sensitivity**	**Specificity**	**F-Score**	**Jaccard Index**
Training Phase (70%)						
Normal	98.98	100.00	98.98	100.00	99.49	98.98
Abnormal	100.00	99.24	100.00	98.98	99.62	99.24
Average	**99.49**	**99.62**	**99.49**	**99.49**	99.55	**99.11**
Testing Phase (30%)						
Normal	100.00	97.87	100.00	98.11	98.92	97.87
Abnormal	98.11	100.00	98.11	100.00	99.05	98.11
Average	**99.06**	**98.94**	**99.06**	**99.06**	**98.99**	**97.99**
Training Phase (60%)						
Normal	100.00	98.73	100.00	99.15	99.36	98.73
Abnormal	99.15	100.00	99.15	100.00	99.57	99.15
Average	**99.58**	**99.37**	**99.58**	**99.58**	**99.47**	**98.94**
Testing Phase (40%)						
Normal	100.00	95.65	100.00	95.38	97.78	95.65
Abnormal	95.38	100.00	95.38	100.00	97.64	95.38
Average	**97.69**	**97.83**	**97.69**	**97.69**	**97.71**	**95.52**

In Figure 5, we see the results of a test of the EOADL-BTSC model's TLS and VLS on the BraTS 2019 dataset. According to the graph, the EOADL-BTSC technique has shown promising results with modest TLS and VLS values. The EOADL-BTSC strategy obviously produces lower VLS results.

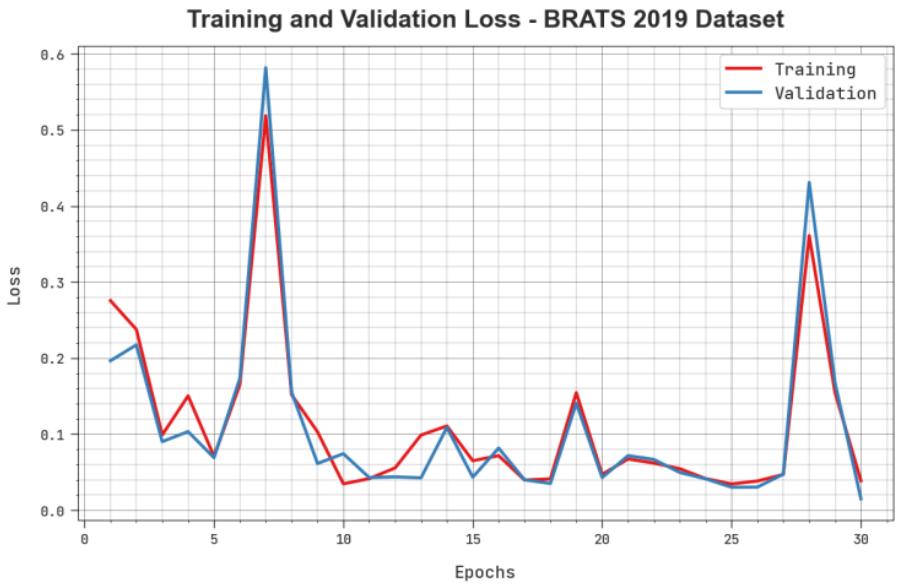

Figure 5. TLS and VLS analysis of EOADL-BTSC system under BraTS 2019 dataset

The confusion matrices created by the EOADL-BTSC method on the BraTS 2020 database are revealed in Figure 6. The results showcase that EOADL-BTSC methodology has properly identified the normal and abnormal BT classes.

Table 3 offers detailed BT classification outcomes of the EOADL-BTSC algorithm on the BraTS 2020 dataset. The outcomes implied the improved efficacy of the EOADL-BTSC model in all classes. For sample, on 70% of TR database, the EOADL-BTSC methodology has attained an average $accu_{bal}$ of 99.49%, PPV of 99.62%, $sens_y$ of 99.49%, $spec_y$ of 99.49%, F_{score} of 99.55%, and JI of 99.11%. In the meantime, on 30% of TS database, the EOADL-BTSC model has attained an average $accu_{bal}$ of 99.06%, PPV of 98.94%, $sens_y$ of 99.06%, $spec_y$ of 99.06%, F_{score} of 98.99%, and JI of 97.99%. Eventually, on 60% of the TR database, the EOADL-BTSC model has attained average $accu_{bal}$ of 99.58%, PPV of 99.37%, $sens_y$ of 99.58%, $spec_y$ of 99.58%, F_{score} of 99.47%, and JI of 98.94%.

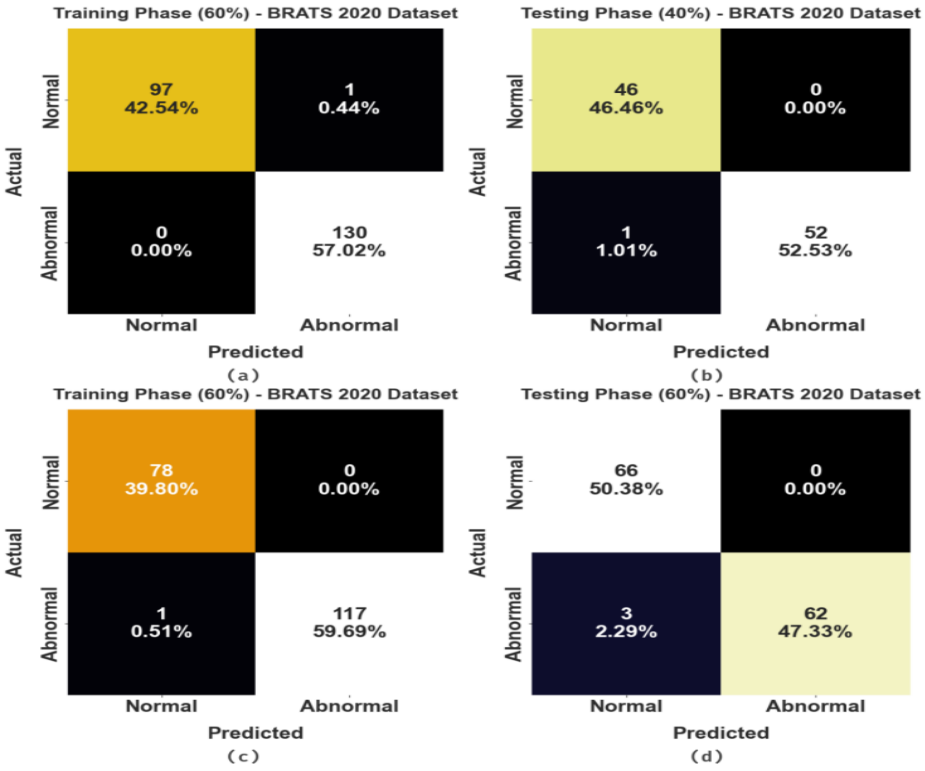

Figure 6. Confusion matrices of EOADL-BTSC system BraTS 2020 dataset (a-b) TR and TS databases of 70:30 and (c-d) TR and TS databases of 60:40.

Table 4. Comparative analysis of EOADL-BTSC approach with other recent methods under BraTS 2019 dataset.

BraTS 2019 Dataset					
Methods	**Accuracy**	**Sensitivity**	**Specificity**	**PPV**	**Jaccard Index**
EOADL-BTSC	99.15	98.78	99.15	99.15	97.93
DT	94.54	94.55	94.83	92.87	94.44
Linear LDA	97.66	98.01	96.25	95.54	96.93
Logistic regression	98.76	98.47	97.32	96.83	97.82
Linear SVM	98.89	98.55	98.80	97.66	96.08
KNN	98.41	97.56	98.68	98.37	97.27
Ensemble	97.30	96.15	98.58	97.80	97.49

Table 5. Comparative analysis of EOADL-BTSC method with other recent techniques under BraTS 2020 database

BraTS 2020 Dataset					
Methods	**Accuracy**	**Sensitivity**	**Specificity**	**PPV**	**Jaccard Index**
EOADL-BTSC	99.58	99.58	99.58	99.37	98.94
DT	93.15	95.72	91.15	88.53	92.07
Linear LDA	98.87	97.18	98.7	98.27	97.76
Logistic regression	99.11	98.99	98.8	98.78	98.24
Linear SVM	97.23	97.18	97.9	97.64	97.41
KNN	98.42	97.77	99.21	99.08	97.97
Ensemble	95.47	95.71	95.78	94.83	96.01

In Figure 7, we see the results of a test of the EOADL-BTSC model's TLS and VLS on the BraTS 2020 dataset. The graph implied that the EOADL-BTSC approach has shown superior performance with low TLS and VLS values. The EOADL-BTSC method obviously produces lower VLS values.

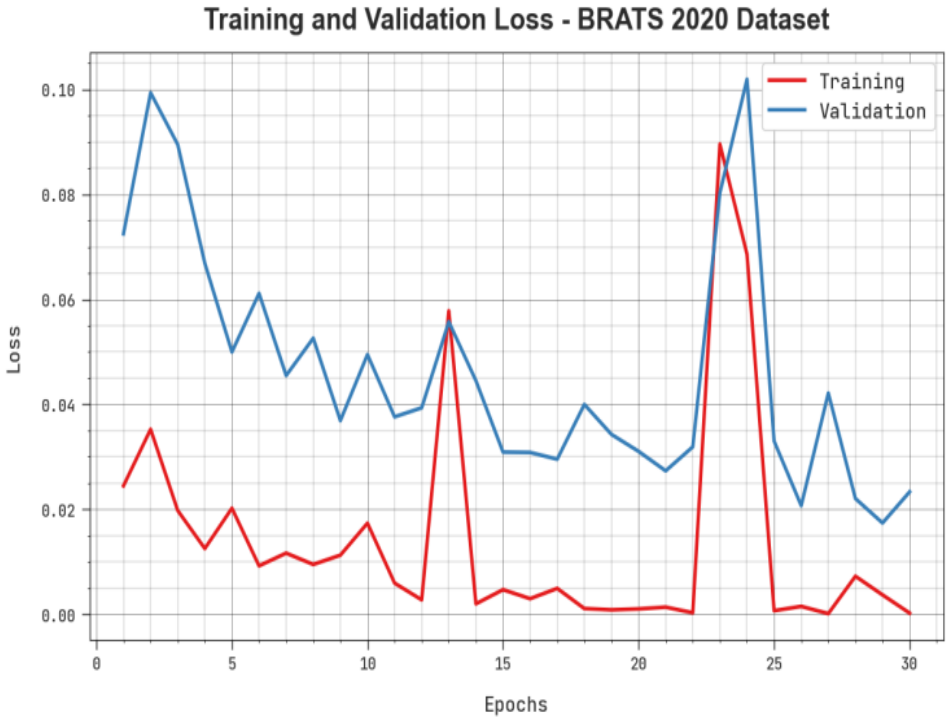

Figure 7. TLS and VLS analysis of EOADL-BTSC system under BraTS 2020 dataset

Table 4 reports an overall comparative analysis of the EOADL-BTSC method with recent techniques on the BraTS 2019 dataset. Table 4 examines the comparative $accu_y$, $sens_y$, $spec_y$,PPV and JI results of the EOADL-BTSC model on the BraTS 2019 database. The table implied that the DT methodology has shown lower values of $accu_y$, $sens_y$, and $spec_y$ values.

Furthermore, the linear LDA and LR methods have achieved slightly increased $accu_y$, $sens_y$, and $spec_y$ values. Although the linear SVM, KNN, and ensemble models have obtained reasonable $accu_y$, $sens_y$, and $spec_y$ values, the EOADL-BTSC model has gained maximum $accu_y$, $sens_y$, and $spec_y$ values of 99.15% 98.78%, and 99.15% respectively.

Table 4 implies that the DT methodology has shown lower values of PPV and JI. Moreover, the linear LDA and LR methods have slightly increased PPV and JI values. Although the linear SVM, KNN, and ensemble models have obtained reasonable PPV and JI values, the EOADL-BTSC model has gained maximum PPV and JI values of 99.15% and 97.93%, respectively.

Table 5 reports an overall analysis of the EOADL-BTSC method with recent methods in the BraTS 2020 database. Table 5 examines the comparative $accu_y$, $sens_y$, $spec_y$,PPV and JI results of the EOADL-BTSC model on the BraTS 2020 database. The table implied that the DT algorithm has shown lower values of $accu_y$, $sens_y$, and $spec_y$ values. Furthermore, the linear LDA and LR methods have reached slightly increased $accu_y$, $sens_y$, and $spec_y$ values. Although the linear SVM, KNN, and ensemble models have obtained reasonable $accu_y$, $sens_y$, and $spec_y$ values, the EOADL-BTSC model has gained maximum $accu_y$, $sens_y$, and $spec_y$ values of 99.58% 99.58%, and 99.58% respectively.

Table 5 implies that the DT approach has shown lower PPV and JI values. Furthermore, the linear LDA and LR methods have achieved increased PPV and JI values. Although the linear SVM, KNN, and ensemble models have obtained reasonable PPV and JI values, the EOADL-BTSC model has gained maximum PPV and JI values of 99.37% and 98.94%, respectively. Thus, the EOADL-BTSC model has shown enhanced performance in the BT classification process.

EOADL-BTSC method can be helpful to society in several ways. Accurate and fast detection of brain tumors can lead to early diagnosis and treatment, which can significantly improve patient outcomes and survival rates.The automatic segmentation of brain tumors in medical images can assist doctors and medical professionals in planning appropriate treatment strategies for patients. This can help in designing more effective treatment plans, reducing the risk of surgical complications, and improving patient outcomes. The time and energy needed for manual examination of medical pictures can be reduced with the help of automated approaches for segmenting and classifying brain tumor utilising deep learning models. This can lead to improved efficiency in medical diagnosis and treatment planning. By enhancing the precision and consistency of brain tumor segmentation and classification, the suggested EOADL-BTSC approach can also help to the development of medical imaging technology. In the long run, this can help patients by paving the way for more research in the field of medical imaging.

CONCLUSION

In this study, a new EOADL-BTSC methodology was formulated for BT segmentation and classification on brain MRI. The presented EOADL-BTSC technique involves different phases of operations such as pre-processing, attention inception-based UNet segmentation, EOA-based parameter tuning, extraction of features through CapsNet model, and CRNN classification. At first, the contrast level of the images is improved, and then skull stripping is performed. Next, the segmentation of MRI is performed by EOA with an attention-inception-based U-Net model. Finally, the CapsNet feature extraction and CRNN classification processes are carried out. To showcase the improved performance of the EOADL-BTSC method, a wide range of simulation analyses were executed using a benchmark dataset. According to the results of the simulations, the EOADL-BTSC technique is superior to other contemporary methods in a number of performance metrics. To improve the EOADL-BTSC algorithm's classification capabilities, a fusion model based on ensemble DL can be created in the near future.

Funding: This research received no external funding.
Conflicts of Interest: The authors declare no conflict of interest.

REFERENCES

1. Pei L, Vidyaratne L, Rahman MM, Iftekharuddin KM. Context aware deep learning for brain tumor segmentation, subtype classification, and survival prediction using radiology images. Sci Rep. 2020 Nov 12;10(1):19726.
2. Yaqub M, Feng J, Zia MS, Arshid K, Jia K, Rehman ZU, Mehmood A. State-of-the-art CNN optimizer for brain tumor segmentation in magnetic resonance images. Brain Sciences. 2020 Jul 3;10(7):427.
3. Karuppusamy P. Hybrid manta ray foraging optimization for novel brain tumor detection. J Soft Computing Paradigm (JSCP). 2020 Jul 23;2(03):175-85.

4. Murthy MY, Koteswararao A, Babu MS. Adaptive fuzzy deformable fusion and optimized CNN with ensemble classification for automated brain tumor diagnosis. Biomedical Engineering letters. 2021 Nov 7:1-22.
5. Muhammad K, Khan S, Del Ser J, De Albuquerque VH. Deep learning for multigrade brain tumor classification in smart healthcare systems: A prospective survey. IEEE Transactions on Neural Networks and Learning Systems. 2020 Jun 30;32(2):507-22.
6. Raja PS. Brain tumor classification using a hybrid deep autoencoder with Bayesian fuzzy clustering-based segmentation approach. Biocybernetics and Biomedical Engineering. 2020 Jan 1;40(1):440-53.
7. Yang T, Song J, Li L. A deep learning model integrating SK-TPCNN and random forests for brain tumor segmentation in MRI. Biocybernetics and Biomedical Engineering. 2019 Jul 1;39(3):613-23.
8. Das S, Bose S, Nayak GK, Satapathy SC, Saxena S. Brain tumor segmentation and overall survival period prediction in glioblastoma multiforme using radiomic features. Concurrency and Computation: Practice and Experience. 2022 Sep 10;34(20):e6501.
9. Deng W, Shi Q, Wang M, Zheng B, Ning N. Deep learning-based HCNN and CRF-RRNN model for brain tumor segmentation. IEEE Access. 2020 Jan 15;8:26665-75.
10. Narmatha C, Eljack SM, Tuka AA, Manimurugan S, Mustafa M. A hybrid fuzzy brain-storm optimization algorithm for the classification of brain tumor MRI images. Journal of ambient intelligence and humanized computing. 2020 Aug 14:1-9.
11. Raza A, Ayub H, Khan JA, Ahmad I, S. Salama A, Daradkeh YI, Javeed D, Ur Rehman A, Hamam H. A hybrid deep learning-based approach for brain tumor classification. Electronics. 2022 Apr 5;11(7):1146.
12. Yin B, Wang C, Abza F. New brain tumor classification method based on an improved version of whale optimization algorithm. Biomedical Signal Processing and Control. 2020 Feb 1;56:101728.
13. Anaraki AK, Ayati M, Kazemi F. Magnetic resonance imaging-based brain tumor grades classification and grading via convolutional neural networks and genetic algorithms. biocybernetics and biomedical engineering. 2019 Jan 1;39(1):63-74.
14. Kumar S, Mankame DP. Optimization driven deep convolution neural network for brain tumor classification. Biocybernetics and Biomedical Engineering. 2020 Jul 1;40(3):1190-204.
15. Hu A, Razmjooy N. Brain tumor diagnosis based on metaheuristics and deep learning. International Journal of Imaging Systems and Technology. 2021 Jun;31(2):657-69.
16. Deb D, Roy S. Brain tumor detection based on hybrid deep neural network in MRI by adaptive squirrel search optimization. Multimedia tools and applications. 2021 Jan;80:2621-45.
17. Raju AR, Suresh P, Rao RR. Bayesian HCS-based multi-SVNN: a classification approach for brain tumor segmentation and classification using Bayesian fuzzy clustering. Biocybernetics and Biomedical Engineering. 2018 Jan 1;38(3):646-60.
18. Afshar P, Mohammadi A, Plataniotis KN. Brain tumor type classification via capsule networks. In2018 25th IEEE international conference on image processing (ICIP) 2018 Oct 7 (pp. 3129-3133). IEEE.
19. Hussein F, Mughaid A, AlZu'bi S, El-Salhi SM, Abuhaija B, Abualigah L, Gandomi AH. Hybrid CLAHE-CNN Deep Neural Networks for Classifying Lung Diseases from X-ray Acquisitions. Electronics. 2022 Sep 27;11(19):3075.
20. Wang H, Xu G, Pan X, Liu Z, Tang N, Lan R, Luo X. Attention-inception-based U-Net for retinal vessel segmentation with advanced residual. Computers & Electrical Engineering. 2022 Mar 1;98:107670.
21. Mohamed B, Mohaisen L, Amin M. Binary Equilibrium Optimization Algorithm for Computing Connected Domination Metric Dimension Problem. Scientific Programming. 2022 Oct 6;2022.
22. Yang B, Bao W, Wang J. Active disease-related compound identification based on capsule network. Briefings in bioinformatics. 2022 Jan;23(1):bbab462.
23. Hang R, Liu Q, Hong D, Ghamisi P. Cascaded recurrent neural networks for hyperspectral image classification. IEEE Transactions on Geoscience and Remote Sensing. 2019 Mar 7;57(8):5384-94.